Mercury anomalies associated with three extinction events (Capitanian Crisis, Latest Permian Extinction, and the Smithian/Spathian Extinction) in NW Pangea

Stephen E. Grasby[1,2*], Benoit Beauchamp[2], David P.G. Bond[3], Paul B. Wignall[4], Hamed Sanei[1,2]

[1] *Geological Survey of Canada, 3303 33rd St. N.W. Calgary AB Canada, T2L 2A7.*

[2] *Department of Geoscience, University of Calgary, Calgary AB Canada.*

[3]*Department of Geography, Environment and Earth Sciences, University of Hull, Hull HU6 7RX,*

United Kingdom

[4]*School of Earth Sciences, University of Leeds, Woodhouse Lane, Leeds LS2 9JT, United*

Kingdom

*Correspondence to: sgrasby@nrcan.gc.ca +1 (403) 292-7111

Abstract

Permian through Early Triassic strata that include a record of three major extinction events (Capitanian Crisis, Latest Permian Extinction, and the Smithian/Spathian Extinction) were examined at the Festningen section, Spitsbergen. Over the ~ 12 Ma record examined, mercury in the sediments shows relatively constant background values of 0.005 to 0.010 μg/g. However, there are notable spikes in Hg concentration, over an order of magnitude above background, associated with the three extinctions. The Hg/TOC ratio shows similar large spikes, indicating that they represent true increase in Hg loading to the environment. We argue that these represent Hg loading events associated with enhanced Hg emissions from large igneous province (LIP) events that are synchronous with the extinctions. The Hg anomalies are consistent across the NW margin of Pangea, indicating widespread mercury loading occured. While this provides utility as a chemostratigraphic marker, the Hg spikes may also indicate loading of toxic metals to the environment that would be a contributing cause to the mass extinction events.

Keywords: mercury, Early Triassic, Latest Permian Extinction, chemostratigraphy

1. Introduction

Mercury (Hg) emissions associated with the emplacement of Large Igneous Provinces (LIPs) were first recognised by (Sanei et al., 2012), who showed a large Hg spike associated with the Siberian Traps eruptions. This event was coincident with the Latest Permian Extinction (LPE), the largest extinction in Earth History that had a devastating impact on both terrestrial and marine ecosystems (Erwin, 2006). High Hg loading associated with the Siberian Traps has been supported by a similar Hg spike at the LPE boundary in Spitsbergen (Grasby et al., 2015). Recurrent Siberian Trap volcanism may have also influenced Hg loading during the Smithian/Spathian Extinction in the Sverdrup Basin (Grasby et al., 2013a). While these initial studies are focused on the sedimentary records from NW Pangea, the global extent of Hg loading related to Siberian Trap volcanism has yet to be demonstrated. However, subsequent work has shown similar Hg anomalies associated with other LIP events such as the Cretaceous–Paleogene transition (Sial et al., 2014; Sial et al., 2013; Silva et al., 2013) related to Deccan Trap volcanism.

Hg is extremely toxic to life. This combined with the ease of transport over long distances and persistence of Hg in the environment makes modern anthropogenic mercury emissions the subject of significant global concern (AMAP, 2011). The two largest natural source of Hg to the environment are volcanic emissions and natural coal combustion (Pirrone et al., 2010). These sources release Hg to the atmosphere where it can be globally transported prior to deposition in terrestrial and marine environments. In the marine environment organic matter and clay minerals scavenge Hg and transports it to the sea floor to become fixed in bottom sediments (Gehrke et al., 2009; Turner et al., 2004; Andren and Harriss, 1975; Lindberg et al., 1975; Cranston and Buckley, 1972). The control of primary productivity on Hg sequestration is shown by the close

53 relationship between sedimentary organic matter and Hg in modern (Sanei et al., 2014; Stern et

54 al., 2009; Outridge et al., 2007), as well as ancient sediments (Grasby et al., 2013a).

55   Modern volcanic eruptions have a significant Hg flux that produce global Hg anomalies

56 (Pyle and Mather, 2003; Schuster et al., 2002; Slemr et al., 1995; Slemr and Scheel, 1998). Hg is

57 sourced from both volcanic gases as well as from rock units intruded by magma (Grasby et al.,

58 2015; Sanei et al., 2015; Sanei et al., 2012). During LIP events emission rates would greatly

59 exceed normal Hg release (Sanei et al., 2012; Grasby et al., 2015), such that the normal marine

60 buffering control on Hg can be potentially overwhelmed (Sanei et al., 2012; Grasby et al., 2013a)

61 and be recorded as a Hg spike in the sediment record. For instance Grasby et al. (2015) estimated

62 that the Siberian Traps may have released up to 9.98 Gg/a Hg, or 400% above modern natural

63 emissions. In comparision, the modern anthropogenic Hg emissions that roughly equal natural

64 are subject of global concern over impact on marine and terrestrial ecosystems. Therefore, Hg

65 anomalies formed at time of LIP eruptions suggest that: 1) Hg could be an effective marker in

66 the geologic record of periods of enhanced volcanic activity, and 2) LIP eruptions could

67 potentially release toxic amounts of Hg to the environment. Such a scenario would add to the

68 variety of kill mechanisms already associated with major volcanic eruptions (Keller and Kerr,

69 2014), as well as providing a direct link between terrestrial and marine extinction.

70   To further the assessment of Hg in the geologic record, we examined the Permian

71 through Early Triassic record at the Festningen section in Spitsbergen (Fig. 1). This well-known

72 location records the LPE (Grasby et al., 2015; Wignall et al., this volume) as well as evidence for

73 the Earlier Capitanian crisis (Bond et al., 2015) and Smithian/Spathian extinction (Wignall et al.,

74 this volume), all of which have been linked to periods of major volcanic activity. Of these recent

75 studies, the Hg record at Festningen has only been examined in a narrow (40 m) zone straddling

76 the LPE boundary (Grasby et al., 2015). In this present paper we examined the Hg record at

77 Festningen over 600 m of section through the Middle Permian to Early Triassic, representing

78 ~12 million years of Earth history.

79

2. Study Area.

81 The Festningen section is located at Kapp Starostin, Spitsbergen (Fig. 1). The ~45° eastward

82 dipping beds occur along a ~7 km low sea-cliff. The section provides a near continuous exposure

83 of Carboniferous to Cenozoic strata, from Kapp Starostin to Festningsdodden, deposited in a

84 distal broad epicontinental shelf setting on the northwestern margin of Pangea (Wignall et al.,

85 1998; Blomeier et al., 2013; Stemmerik and Worsley, 2005). During Permian time Spitsbergen

86 was at a paleolatitude of ~40-45° N (Scotese, 2004; Golonka and Ford, 2000).

87   The Kapp Starostin Formation was deposited during a period of passive subsidence that

88 followed a major relative sea level drop at the Lower/Middle Permian boundary (Blomeier et al.,

89 2013). Deposition of widespread heterozoan carbonate (Vøringen Member) occurred in Roadian

90 time, followed by the progradation of heterozoan carbonates and cherts over much of the Barents

91 Shelf and Svalbard (Blomeier et al., 2013). Spitsbergen shares a similar depositional history to

92 the palaeogeographically adjoining Sverdrup Basin (van Hauen, Degerböls and Trold Fiord

93 formations; Beauchamp et al., 2009) (Fig. 2). Approximately 40 m below the contact with the

94 overlying uppermost Permian–Lower Triassic Vardebukta Formation, fossiliferous carbonates of

95 the Kapp Starostin Formation transition to Late Permian spiculitic chert (Blomeier et al., 2013).

96 These Later Permian chert beds are considered equivalent to the Black Stripe and Lindström

97 formations of the Sverdrup Basin (Beauchamp et al., 2009). The Vardebukta and overlying

98 Tvillingodden formations are dominated by shale, siltstone and minor sandstone of Early to

99 Middle Triassic age (Mørk et al., 1982), that are equivalent to the Blind Fiord Formation of the

100 Sverdrup Basin (Embry, 1989). The basal ~6-7 m of the Vardebukta Formation is latest Permian

101 in age (Grasby et al., 2015; Wignall et al., 1998).

102

3. Methods

104 A detailed sample suite was collected from 100 m below the Kapp Starostin/Vardebukta contact

105 to 500 m above. Sample spacing varied from 1 to 2 m away from the contact and higher density

106 of 20 to 50 cm spacing from ~ 40 m below to 19 m above the top of the Kapp Starostin

107 Formation. Samples were recorded in metres above (positive) and below (negative) the last chert

108 bed that defines the top of the Kapp Starostin Formation. Weathered surfaces were removed and

109 then samples were collected from an isolated layer no greater than 2 cm thick. In the laboratory

110 any remaining weathered surfaces were removed and fresh samples were powdered by agate

111 mortar and pestle.

112   Total organic carbon (TOC) was measured using Rock-Eval $6^{©}$, with ± 5% analytical error

113 of reported value, based on repeats and reproducibility of standards run after every 5th sample

114 (Lafargue et al., 1998). Elemental determinations were conducted on powdered samples digested

115 in a 2:2:1:1 acid solution of H_2O-HF-$HClO_4$-HNO_3, and subsequently analysed using a

116 PerkinElmer Elan 9000 mass spectrometer, with ± 2% analytical error. Hg was measured at

117 GSC-Atlantic by LECO® AMA254 mercury analyzer (Hall and Pelchat, 1997) (± 10%). $\delta^{13}C_{org}$

118 was determined on samples washed with hydrochloric acid, and rinsed with hot distilled water to

119 remove any carbonate. $\delta^{13}C$ was measured using Continuous Flow-Elemental Analysis-Isotope

120 Ratio Mass Spectrometry, with a Finnigan Mat Delta+XL mass spectrometer interfaced with a

121 Costech 4010 elemental analyzer with combined analytical and sampling error of ± 0.2‰.

122   Analytical results from a total of 341 samples used in this study are provided in Table 1.

123

4. Results

125

4.a. Organic Carbon

127 The organic carbon record, expressed as percent TOC, shows low values (< 1% TOC) overall

128 (Fig. 3a). There is an increase in TOC at –40 m. Bond et al. (2015) argue, based on brachiopod,

129 Sr isotopes records and magnetostratigraphy data, that the –40 m level is around the Middle

130 Permian extinction level at Festningen. The TOC values decline again leading up to the LPE

131 boundary, where there is a second brief increase in TOC just above the LPE. For the remainder

132 of the section, TOC values in the Vardebukta Formation are < 0.2%. At these low values the

133 accuracy of Rockeval results decreases, however data are plotted in Figure 3a to illustrate the

134 overall low TOC values through this interval. The TOC values increase again in the basal

135 Tvillingodden Formation, before dropping to low values in the upper 100 m of section.

136   Rock-Eval 6$^{©}$ results also provided information on thermal maturation and indicated that

137 organic matter in the shales have never been heated past the upper end of the oil window, such

138 that stable isotope values of organic carbon would not be thermally altered (Hayes et al., 1983).

139 The only exception is a local thermal anomaly associated with a sill emplaced at ~19 m that does

140 not extend beyond 5 m of the sill boundary (Grasby et al., 2015).

141

4.b. Carbon isotope record

143 Portions of the organic carbon isotope curve ($\delta^{13}C_{org}$) at the Festningen section have been

144 reported in previous studies, including Middle to Late Permian sediments (Bond et al., 2015),

145 across the Latest Permian extinction event (Grasby et al., 2015) and early Triassic sediments

146 (Wignall et al., this volume). The combined $\delta^{13}C_{org}$ curve is provided here (Fig. 3b) as reference

147 for comparison with both organic carbon isotope data from NW Pangea and the global inorganic

148 carbon isotope record. The $\delta^{13}C_{org}$ data from Festningen shows initially relatively stable values

149 of ~–24 ‰ through the Middle to Late Permian, with a relatively minor negative shift at ~–40 m.

150 At the top of the Kapp Starostin Formation, carbon isotope values show the onset of a

151 pronounced 10‰ negative shift through the basal Vardebukta Formation sediments (Grasby et

152 al., 2015). After this point there is a progressive recovery through the next 200 m followed by

153 another progressive negative shift to a minimum at ~+300 m which is followed by an unstable

154 period through the remainder of the measured section (Wignall et al., this volume).

155

4.c. Molybdenum

157 Similar to the carbon isotope record, trace element data has been shown as a proxy for anoxia for

158 the 3 separate portions of the section previously studied (Grasby et al., 2015; Bond et al., 2015;

159 Wignall et al., this volume). For reference the composite curve of Mo normalised to Al is shown

160 through the entire interval (Fig. 3c). Results show relatively low values at the base of the section

161 with a significant spike in Mo/Al at ~ –40 m, which coincides with the shift to higher TOC

162 values and minor negative shift in $\delta^{13}C_{org}$. Above the LPE boundary there is a second spike in

163 Mo/Al that initiates ~5 m after the main LPE event. This is followed by a gradual decline in

164 Mo/Al until ~200 m, coincident with the reversal in the trend of carbon isotopes. The Mo/Al

165 values progressively increase again through the next 100 m until +300 m, where peak Mo/Al

166 ratios are coincident with the minimum in $\delta^{13}C_{org}$ values. After this Mo/Al values become highly

167 variable for the rest of the measured section.

168

4.d. Mercury

170 Hg values, reported here for the first time, are plotted in Figure 3d. Hg values are 0.005 to 0.010

171 μg/g in the basal 60 m of section and then show a shift above –40 m to values up to 0.050 μg/g,

172 followed by a subsequent decline to values of ∼ 0.020 μg/g in the 10 m below just the LPE

173 boundary. At the LPE there is a significant spike in Hg to the highest values observed in the

174 section (> 0.130 μg/g). Hg concentrations drop rapidly to background values of 0.005 to 0.010

175 μg/g through the remainder of the section. The only exception is a brief spike at ∼+300 m, where

176 Hg concentrations up to 0.065 μg/g are observed.

177 In both marine and freshwater environments dissolved Hg has been shown to have strong

178 affinity for organic matter (OM) (Gehrke et al., 2009; Mason et al., 1996; Han et al., 2006;

179 Gagnon et al., 1997; Benoit et al., 2001). Grasby et al. (2013a) have also shown that OM

180 strongly controls Hg sequestration over geologic time. Therefore, along with absolute

181 concentrations, the Hg/TOC ratio is plotted in Figure 3e. However, TOC values are too low to be

182 considered accurate for parts of the section, where Rockeval analyses cannot accurately resolve

183 concentrations <0.2% TOC. Therefore only samples with TOC > 0.2% are plotted as lower

184 accuracy can greatly affect the calculated ratio. These data show a general trend whereby the

185 Hg/TOC ratio has constant low values through the section. The exceptions to this are the large

186 spikes in Hg/TOC values that occur at the LPE boundary as well as smaller shifts that occur at –

187 40 m as well as at ∼+300 m. These increases in Hg/TOC ratio are consistent with zones where

188 there are large spikes in absolute Hg concentration. Outside of these three levels Hg values are

189 low.

190

5. Discussion

5.a. Carbon isotope chemostratigraphy

The $\delta^{13}C$ record through Permian to Early Triassic sediments shows significant shifts that are comparable to those observed in the Sverdrup Basin (Grasby et al., 2013b) as well as with inorganic $\delta^{13}C$ trends from records in the Panthalassa (Horacek et al., 2009) and the Tethys (Horacek et al., 2007; Payne et al., 2004). This demonstrates that Festningen records global variation in biogeochemical cycles through this time interval. These can be used as a chemostratigraphic tool to support both regional and global correlation.

Bond et al. (2015) argued that the minor negative carbon anomaly at – 40 m correlates with the Capitanian crises. The LPE event, as marked by the loss of chert forming siliceous sponges is characterised by the onset of a large negative shift in $\delta^{13}C_{org}$ that reaches a minimum in the basal Vardebukta Formation (Grasby et al., 2015; Wignall et al., 1998). Above the Kapp Starostin Formation Wignall et al. (this volume) show that the next negative low point at ~300 m is correlative with the end Smithian Substage. This is also consistent with comparison to the $\delta^{13}C_{org}$ record from the Smithian stratotype (Grasby et al., 2013b), as illustrated in Figure 4. This makes the low in carbon isotope values equivalent to the Smithian/Spathian Extinction event that was associated with renewed Siberian Trap volcanism and rapid global temperature increase (Brayard et al., 2006; Orchard, 2007; Sun et al., 2012; Xie et al., 2010).

5.b. Mercury deposition

The Hg record at Festningen shows a relatively constant background value through the majority of the succession analysed (< 0.020 µg/g). However notable spikes in Hg concentration occur coincident with the three extinction levels represented in this section (Capitanian Crisis, LPE,

214 and Smithian/Spathian Extinction). Of these three spikes the most significant occurs at the LPE

215 boundary. Aside from the three most prominent Hg spikes there is also a slight increase in late

216 Dienerian portion of the section. It is interesting to note that these prominent Hg spikes are all

217 associated with shifts to lower $\delta^{13}C$ values. In addition there is a general association of higher Hg

218 concentrations associated with high Mo/Al values (Fig. 2). While this may suggest increased Hg

219 sequestration associated with changes to more anoxic environments, a plot of Mo/Al versus Hg

220 reveals that there is no correlation (Fig. 5). So despite the general relationship, the data suggest

221 that anoxia has no direct influence on Hg sequestration in sediments.

222　　　Given the low organic matter content, throughout much of the Early Triassic portion of the

223 studied section, reliable Hg/TOC ratios are not always possible to obtain. For values <0.2% TOC

224 inaccuracies in measurement can lead to magnified errors and highly variable Hg/TOC values

225 that are not reflective of natural conditions, and therefore not shown. However, for TOC values >

226 0.2%, the Hg/TOC ratios for the Festningen section have relatively constant background values

227 (vertical dashed line in Fig. 2e). These results are consistent with Hg/TOC through the Early

228 Triassic at the Smithian stratotype, Sverdrup Basin (Grasby et al., 2013a), indicating a general

229 background level of Hg sequestration into sediment that is largely controlled by organic matter

230 deposition.

231　　　The notable exceptions to this background Hg deposition are spikes in both total Hg

232 concentrations as well as Hg/TOC levels at the 3 extinction levels (Fig. 2). Previously Sanei et

233 al. (2012) and (Grasby et al., 2013a) have argued that Hg anomalies in the geologic record are

234 related to massive Hg emissions associated with periods of major volcanic eruptions. Our results

235 from Festningen provide support for this hypothesis, showing over the ~12 ma record that there

236 are three prominent Hg anomalies superimposed on background Hg concentrations. In each case

237 these Hg spikes are associated with global extinction events that have been previously tied to LIP

238 eruptions: Capitanian Crisis - Emeishan eruptions, LPE – Siberian Traps, Smithian/Spathian –

239 renewed Siberian Traps (Bond and Wignall, 2014; Xie et al., 2010; Paton et al., 2010).

240 On a regional perspective the Hg spikes observed at Festningen closely correspond to those

241 in the Sverdrup Basin (Fig. 4). This indicates that these periods of anomalous Hg deposition are

242 regional in scope and suggest periods of enhanced Hg deposition over broad areas.

243

6. Conclusions

245 The organic carbon isotope records from the Festningen section show trends through the Late

246 Permian and Early Triassic that closely correspond to those of the Sverdrup Basin, as well as the

247 global inorganic carbon record. These results illustrate that NW Pangea records perturbations to

248 the global carbon cycle. Previously it has been demonstrated that Hg is an excellent proxy for

249 periods of major volcanic activity in the geologic record (Sanei et al., 2012; Grasby et al., 2013a;

250 Sial et al., 2013). The Festningen section records a general constant background of Hg deposition

251 through time. However, there are notable spikes in Hg concentration as well as in the Hg/TOC

252 ratio that correspond to periods of mass extinction (Capitanian Crisis, the LPE event, and the

253 Smithian/Spathian extinction), all of which have been associated with LIP events. Our results

254 thus support the use of Hg as a marker for LIP eruptions. What remains uncertain is what role

255 such Hg release could have on ecosystems. Certainly Hg is one of the most toxic elements for

256 life, and enhanced Hg flux from large igneous events would likely have global impact in both the

257 terrestrial and marine realm. Our results show that there are consistent records of Hg spikes

258 associated with LIP events and mass extinctions across NW Pangea. The global nature of these

259 records remains to be demonstrated. If they are more widely distributed then Hg release could

260 have played a role as a significant extinction mechanism throughout Earth history.

261

Acknowledgments

269

Figure Legends

271 Figure 1. Map showing location of the Festningen section on Spitsbergen (base of section is

272   located at 78.0950°N, 13.8240°E (WGS84 datum).

273 Figure 2. Paleogeographic map after (Embry, 1992) showing relative location of Sverdrup Basin

274   and Spitsbergen. Inset map (after Scotese) showing location on NW Pangea.

275 Figure 3. Plots of geochemical data from Festningen, showing: a) percent total organic carbon

276   (TOC), b) carbon isotope values for organic carbon, c) Mo normalised by Al, d) Hg

277   values, and e) Hg normalised by TOC (the Hg/TOC values are only shown for values

278   of TOC > 0.2% as below that value Rockeval analyses provide less accurate results

279   that are magnified in calculated ratios).

280 Figure 4. Correlation of carbon isotope and Hg records from the Smithian stratotype (Grasby et

281   al., 2013b) with composite record from Festningen (this study).

282 Figure 5. Plot of the Mo/Al ratio versus Hg concentration.

283

References

AMAP 2011. *AMAP Assessment 2011: Mercury in the Arctic*. Oslo, Norway: Arctic Monitoring and Assessment Programme (AMAP).

ANDREN, A. W. & HARRISS, R. C. 1975. Observations on the association between mercury and organic matter dissolved in natural waters. *Geochimica et Cosmochimica Acta* 39(9), 1253–58.

BEAUCHAMP, B., HENDERSON, C. M. B., GRASBY, S. E., GATES, L., BEATTY, T., UTTING, J. & JAMES, N. P. 2009. Late Permian sedimentation in the Sverdrup Basin, Canadian Arctic: the Lindström and Black Stripe formations. *Canadian Society of Petroleum Geology Bulletin* 57, 167–91.

BENOIT, J. M., MASON, R. P., GILMOUR, C. C. & AIKEN, G. R. 2001. Constants for mercury binding by dissolved organic matter isolates from the Florida Everglades. *Geochimica et Cosmochimica Acta* 65(24), 4445–51.

BLOMEIER, D., DUSTIRA, A. M., FORKE, H. & SCHEIBNER, C. 2013. Facies analysis and depositional environments of a storm-dominated, temperate to cold, mixed siliceous-carbonate ramp: the Permian Kapp Starostin Formation in NE Svalbard. *Norwegian Journal of Geology* 93, 75–98.

BOND, D. P. G., WIGNALL, P. B., JOACHIMSKI, M., SUN, Y., SAVOV, I., GRASBY, S. E., BEAUCHAMP, B. & BLOMEIER, D. P. G. 2015. An abrupt extinction in the Middle Permian (Capitanian) of the Boreal Realm (Spitsbergen). Geological Society of America Bulletin. doi: 10.1130/B31216.1

305 BOND, D. P. G. & WIGNALL, P. B. 2014. Large igneous provinces and mass extinctions: An

306   update. In *Volcanism, Impacts, and Mass Extinctions: Causes and Effects* eds G. Keller

307   and A. C. Kerr). GSA SPECIAL PAPERS, V. 505, DOI:10.1130/2014.2505(02).

308 BRAYARD, A., BUCHER, H., ESCARGUEL, G., FLUTEAU, F., BOURQUIN, S. & GALFETTI, T. 2006.

309   The Early Triassic ammonoid recovery: Paleoclimatic significance of diversity gradients.

310   *Palaeogeography, Palaeoclimatology, Palaeoecology* 239(3–4), 374–95.

311 CRANSTON, R. E. & BUCKLEY, D. E. 1972. Mercury pathways in a river and estuary.

312   *Environmental Science & Technology* 6(3), 274–78.

313 EMBRY, A. 1989. Correlation of Upper Palaeozoic and Mesozoic sequences between Svalbard,

314   Canadian Arctic Archipelago, and northern Alaska. In *Correlation in Hydrocarbon*

315   *Exploration* (ed J. D. Collinson). pp. 89–98. Springer Netherlands.

316 EMBRY, A. F. 1992. Crockerland-The Northwest source area for the Sverdrup Basin, Canadian

317   Arctic Islands. In *Arctic Geology and Petroleum Potential* eds T. O. Vorren, E. Bergsager,

318   Ø. A. Dahl-Stamnes, E. Holter, B. Johansen, E. Lie and T. B. Lund). pp. 205–16.

319   Amsterdam: Elsevier.

320 ERWIN, D. H. 2006. *Extinction. How life on Earth nearly ended 250 million years ago*. New

321   Jersey: Princeton University Press.

322 GAGNON, C., PELLETIER, É. & MUCCI, A. 1997. Behaviour of anthropogenic mercury in coastal

323   marine sediments. *Marine Chemistry* 59(1–2), 159–76.

324 GEHRKE, G. E., BLUM, J. D. & MEYERS, P. A. 2009. The geochemical behavior and isotopic

325   composition of Hg in a mid-Pleistocene western Mediterranean sapropel. *Geochimica et*

326   *Cosmochimica Acta* 73(6), 1651–65.

327 GOLONKA, J. & FORD, D. 2000. Pangean (Late Carboniferous–Middle Jurassic)

328   paleoenvironment and lithofacies. *Palaeogeography, Palaeoclimatology, Palaeoecology*

329   161, 1–34.

330 GRASBY, S. E., BEAUCHAMP, B., BOND, D. P. G., WIGNALL, P. B., TALAVERA, C., GALLOWAY, J.

331   M., PIEPJOHN, K., REINHARDT, L. & BLOMEIER, D. 2015. Progressive environmental

332   deterioration in NW Pangea leading to the Latest Permian Extinction. *Geological Society*

333   *of America Bulletin*.

334 GRASBY, S. E., SANEI, H., BEAUCHAMP, B. & CHEN, Z. 2013a. Mercury deposition through the

335   Permo–Triassic Biotic Crisis. *Chemical Geology* 351(0), 209–16.

336 GRASBY, S. E., BEAUCHAMP, B., EMBRY, A. F. & SANEI, H. 2013b. Recurrent Early Triassic

337   ocean anoxia. *Geology* 41, 175–78.

338 HALL, G. & PELCHAT, P. 1997. Evaluation of a Direct Solid Sampling Atomic Absorption

339   Spectrometer for the Trace Determination of Mercury in Geological Samples. *Analyst*

340   122(9), 921–24.

341 HAN, S., GILL, G. A., LEHMAN, R. D. & CHOE, K.-Y. 2006. Complexation of mercury by

342   dissolved organic matter in surface waters of Galveston Bay, Texas. *Marine Chemistry*

343   98(2-4), 156–66.

344 HAYES, J. M., KAPLAN, I. R. & WEDEKING, K. W. 1983. In *Earth's earliest biosphere: its origin*

345   *and evolution* (ed J. W. Schopf). pp. 92–132. Princeton NJ: Princeton Univ. Press.

346 HORACEK, M., KOIKE, T. & RICHOZ, S. 2009. Lower Triassic [delta]13C isotope curve from

347   shallow-marine carbonates in Japan, Panthalassa realm: Confirmation of the Tethys

348   [delta]13C curve. *Journal of Asian Earth Sciences* 36(6), 481–90.

349   HORACEK, M., BRANDNER, R. & ABART, R. 2007. Carbon isotope record of the P/T boundary and

350   the Lower Triassic in the Southern Alps: Evidence for rapid changes in storage of organic

351   carbon. *Palaeogeography, Palaeoclimatology, Palaeoecology* 252(1–2), 347–54.

352   KELLER, G. & KERR, A. C., eds. 2014. *Volcanism, Impacts, and Mass Extinctions: Causes and*

353   *Effects*. Geological Society of America.

354   LAFARGUE, E., ESPITALITE, J., MARQUIS, F. & PILLOT, D. 1998. Rock-Eval 6 applications in

355   hydrocarbon exploration, production and soil contamination studies. *Revue de L'institut*

356   *Francais du Petrole* 53(4), 421–37.

357   LINDBERG, S. E., ANDRENSON, A. W. & HARRISSON, R. C. 1975. Geochemistry of mercury in the

358   estuarine environment. In *Estuarine Research. Chemistry, Biology and the Estuarine*

359   *System* (ed E. L. Cronin). New York: Cronin. Academic Press.

360   MASON, R. P., REINFELDER, J. R. & MOREL, F. M. M. 1996. Uptake, Toxicity, and Trophic

361   Transfer of Mercury in a Coastal Diatom. *Environmental Science & Technology* 30(6),

362   1835–45.

363   MØRK, A., KNARUD, R. & WORSLEY, D. 1982. Depositional and diagenetic environments of the

364   Triassic and Lower Jurassic succession of Svalbard. In *Arctic geology and geophysics:*

365   *proceedings of the Third International Symposium on Arctic Geology* eds A. F. Embry and

366   H. R. Balkwill). pp. 371–98. Calgary: Canadian Society of Petroleum Geologists.

367   ORCHARD, M. J. 2007. Conodont diversity and evolution through the latest Permian and Early

368   Triassic upheavals. *Palaeogeography, Palaeoclimatology, Palaeoecology* 252(1–2), 93–

369   117.

370 OUTRIDGE, P. M., SANEI, H., STERN, G. A., HAMILTON, P. B. & GOODARZI, F. 2007. Evidence for

371   control of mercury accumulation in sediments by variations of aquatic primary productivity

372   in Canadian High Arctic lakes. . *Environmental Science & Technology* 41, 5259–65.

373 PATON, M. T., IVANOV, A. V., FIORENTINI, M. L., MCNAUGHTON, N. J., MUDROVSKA, I.,

374   REZNITSKII, L. Z. & DEMONTEROVA, E. I. 2010. Late Permian and Early Triassic magmatic

375   pulses in the Angara-Taseeva syncline, Southern Siberian Traps and their possible

376   influence on the environment. *Russian Geology and Geophysics* 51(9), 1012–20.

377 PAYNE, J. L., LEHRMANN, D., J., WEI, J., ORCHARD, M. J., SCHRAG, D. P. & KNOLL, A. H. 2004.

378   Large perturbations of the carbon cycle during recovery from the End-Permian extinction.

379   *Science* 305, 506–09.

380 PIRRONE, N., CINNIRELLA, S., FENG, X., FINKELMAN, R. B., FRIEDLI, H. R., LEANER, J., MASON,

381   R., MUKHERJEE, A. B., STRACHER, G. B., STREETS, D. G. & TELMER, K. 2010. Global

382   mercury emissions to the atmosphere from anthropogenic and natural sources. *Atmospheric*

383   *Chemistry and Physics Discussions* 10, 4719–52.

384 PYLE, D. M. & MATHER, T. A. 2003. The importance of volcanic emissions for the global

385   atmospheric mercury cycle. *Atmospheric Environment* 37(36), 5115–24.

386 SANEI, H., GRASBY, S. E., & BEAUCHAMP, B. 2015. CONTAMINANTS IN MARINE SEDIMENTARY

387   DEPOSITS FROM COAL FLY ASH DURING THE LATEST PERMIAN EXTINCTION (BOOK CHAPTER

388   5), IN: ENVIRONMENTAL CONTAMINANTS: USING NATURAL ARCHIVES TO TRACK SOURCES

389   AND LONG-TERM TRENDS OF POLLUTION, SERIES: DEVELOPMENTS IN

390   PALEOENVIRONMENTAL RESEARCH, VOL. 18, BY: BLAIS, JULES M., ROSEN, MICHAEL R.,

391   SMOL, JOHN P., SPRINGER, P 547, ISBN 978-94-017-9540-1.

392   Sanei, H., Outridge, P. M., Stern, G. A., & Macdonald, R. W. 2015.Classification of mercury-

393   labile organic matter relationships in lake sediments. Chemical Geology, 373, 87–92.

394

395   SANEI, H., GRASBY, S. E. & BEAUCHAMP, B. 2012. Latest Permian mercury anomalies. *Geology*

396   40(1), 63–66.

397   SCHUSTER, P. F., KRABBENHOFT, D. P., NAFTZ, D. L., CECIL, L. D., OLSON, M. L., DEWILD, J. F.,

398   SUSONG, D. D., GREEN, J. R. & ABBOTT, M. L. 2002. Atmospheric Mercury Deposition

399   during the Last 270 Years: A Glacial Ice Core Record of Natural and Anthropogenic

400   Sources. *Environmental Science & Technology* 36(11), 2303–10.

401   SCOTESE, C. R. 2004. A continental drift flipbook. *Journal of Geology* 112, 729–41.

402   SIAL, A. N., CHEN, J., LACERDA, L. D., PERALTA, S., GAUCHER, C., FREI, R., CIRILLI, S.,

403   FERREIRA, V. P., MARQUILLAS, R. A., BARBOSA, J. A., PEREIRA, N. S. & BELMINO, I. K. C.

404   2014. High-resolution Hg chemostratigraphy: A contribution to the distinction of chemical

405   fingerprints of the Deccan volcanism and Cretaceous–Paleogene Boundary impact event.

406   *Palaeogeography, Palaeoclimatology, Palaeoecology* 414(0), 98–115.

407   SIAL, A. N., LACERDA, L. D., FERREIRA, V. P., FREI, R., MARQUILLAS, R. A., BARBOSA, J. A.,

408   GAUCHER, C., WINDMÖLLER, C. C. & PEREIRA, N. S. 2013. Mercury as a proxy for volcanic

409   activity during extreme environmental turnover: The Cretaceous–Paleogene transition.

410   *Palaeogeography, Palaeoclimatology, Palaeoecology* 387(0), 153–64.

411   SILVA, M. V. N., SIAL, A. N., BARBOSA, J. A., FERREIRA, V. P., NEUMANN, V. H. & DE LACERDA,

412   L. D. 2013. Carbon isotopes, rare-earth elements and mercury geochemistry across the K–

413   T transition of the Paraíba Basin, northeastern Brazil. *Geological Society, London, Special*

414   *Publications* 382.

415 SLEMR, F. & SCHEEL, H. E. 1998. Trends in atmospheric mercury concentrations at the summit of

416   the Wank mountain, Southern Germany. *Atmospheric Environment* 32(5), 845–53.

417 SLEMR, F., JUNKERMANN, W., SCHMIDT, R. W. H. & SLADKOVIC, R. 1995. Indication of change in

418   global and regional trends of atmospheric mercury concentrations. *Geophysical Research*

419   *Letters* 22(16), 2143–46.

420 STEMMERIK, L. & WORSLEY, D. 2005. 30 years on - Arctic Upper Palaeozoic stratigraphy,

421   depositional evolution and hydrocarbon prospectivity. *Norsk Geologisk Tidsskrift* 85, 151–

422   68.

423 STERN, G. A., SANEI, H., ROACH, P., DELARONDE, J. & OUTRIDGE, P. M. 2009. Historical

424   interrelated variations of mercury and aquatic organic matter in lake sediment cores from a

425   subarctic lake in Yukon, Canada: further evidence toward the algal-mercury scavenging

426   hypothesis. *Environ. Sci. Technol* 43, 7684–90.

427 SUN, Y., JOACHIMSKI, M. M., WIGNALL, P. B., YAN, C., CHEN, Y., JIANG, H., WANG, L. & LAI, X.

428   2012. Lethally Hot Temperatures During the Early Triassic Greenhouse. *Science*

429   338(6105), 366–70.

430 TURNER, A., MILLWARD, G. E. & LE ROUX, S. M. 2004. Significance of oxides and particulate

431   organic matter in controlling trace metal partitioning in a contaminated estuary. *Marine*

432   *Chemistry* 88(3–4), 179–92.

433 WIGNALL, P. B., BOND, D. P. G., SUN, Y., GRASBY, S. E., BEAUCHAMP, B., JOACHIMSKI, M. &

434   BLOMEIER, D. this volumne. Ultra-Shallow Marine Anoxia in an Early Triassic Storm-

435   Dominated Clastic Ramp (Spitsbergen) and the Suppression of Benthic Radiation.

436   *Geological Magazine*.

437   WIGNALL, P. B., MORANTE, R. & NEWTON, R. 1998. The Permo–Triassic transition in

438   Spitsbergen: $\delta^{13}C_{org}$ chemostratigraphy, Fe and S geochemistry, facies, fauna and trace

439   fossils. *Geologic Magazine* 135, 47–62.

440   XIE, S., PANCOST, R. D., WANG, Y., YANG, H., WIGNALL, P. B., LUO, G., JIA, C. & CHEN, L. 2010.

441   Cyanobacterial blooms tied to volcanism during the 5 m.y. Permo–Triassic biotic crisis.

442   *Geology* 38(5), 447–50.

443

444

Table 1. Geochemical data from the Festningen section. Depths are measured relative to the Latest Permian Extintion Boundary (LPE) marked by the top of the Kapp Starostin Formation.

Sample ID	depth realtive to LPE metres	$\delta^{13}C$ org ‰	Hg ppb	TOC %	Mo PPM	Al %
C-556979	-97.7	-24.5	9	0.02	0.45	0.54
C-556980	-97.2	-21.0	5	0.07	0.48	0.31
C-556981	-95.7	-22.2	4	0.05	0	0.59
C-556982	-94.2	n.d.	5	0.04	0	0.58
C-556983	-92.7	-22.4	6	0.11	0.09	1.02
C-556984	-91.2	-23.0	2	0.01	0.05	0.42
C-556985	-89.7	-23.0	2	0.02	0.07	0.3
C-556986	-86.7	-25.0	11	0.22	0.31	1.59
C-556987	-83.7	-24.0	7	0.11	0.2	1.15
C-556988	-80.7	-23.7	5	0.02	0.08	0.6
C-556989	-77.7	-25.0	6	0.03	0.22	0.61
C-556990	-74.7	-23.8	9	0.12	0.1	1.55
C-556991	-71.7	-24.3	6	0.02	0	0.53
C-556992	-68.7	-24.5	4	0.02	0	0.71
C-556993	-65.7	-25.5	4	0.05	0	0.64
C-556994	-62.7	-24.4	4	0.01	0	0.85
C-556995	-59.7	-24.8	4	0.03	0.08	0.59
C-556996	-56.7	-24.6	4	0.07	0.09	0.75
C-556997	-53.7	-25.2	4	0.07	0.21	1.21
C-556998	-50.7	-25.3	3	0.10	0	1.01
C-556999	-47.7	-24.5	4	0.01	0	0.7
C-557000	-46.2	-24.9	9	0.09	0.13	1
C-557001	-44.7	-24.5	6	0.05	0.13	1.28
C-557002	-43.2	-24.2	5	0.03	0.08	0.9
C-557003	-41.7	-23.6	6	0.08	0.06	0.45
C-557004	-40.2	-23.3	7	0.04	0.2	1.55
C-556572	-27.2	-24.3	28	0.25	0.53	2.65
C-556573	-26.7	-24.6	34	0.44	0.82	4.18
C-556574	-26.2	-24.6	36	0.39	0.99	3.85
C-556575	-25.7	-24.4	22	0.33	0.57	3.63
C-556576	-25.2	-24.7	22	0.29	2.66	2.84
C-556577	-24.7	-24.5	17	0.22	1.05	2.6
C-556578	-24.2	-24.4	35	0.34	1.83	3.3
C-556579	-23.7	-24.0	41	0.43	0	
C-556580	-23.2	-23.8	34	0.49	0.34	3.68
C-556581	-22.2	-23.74	48	0.65	0.25	4.36
C-556582	-21.7	-23.6	42	0.69	0.39	4.43

C-556583	-21.2	-23.63	38	0.59	0.26	4.21
C-556584	-20.7	-23.87	30	0.60	0.48	4.26
C-556585	-20.2	-23.62	37	0.58	0.46	4.54
C-556586	-19.7	-23.6	33	0.55	0.46	4.67
C-556587	-18.2	-23.86	28	0.51	0.8	4.19
C-556588	-17.7	-23.88	30	0.50	0.97	4.18
C-556589	-17.2	-23.9	33	0.57	1.26	3.97
C-556590	-16.7	-23.7	28	0.45	0.52	3.69
C-556591	-16.2	-24.0	29	0.49	0.7	4.2
C-556592	-15.7	-23.3	31	0.45	0.66	4.62
C-556593	-15.2	-24.0	30	0.53	0.74	4.08
C-556594	-14.7	-23.6	30	0.41	0.34	4.35
C-556595	-14.2	-24.1	32	0.44	0.33	4.07
C-556596	-13.7	-23.9	38	0.65	0.22	5.28
C-556597	-13.2	-23.7	34	0.50	0.31	4.7
C-556598	-12.7	-24.0	33	0.48	0.63	4.7
C-556599	-12.2	-24.3	37	0.56	0.57	5.4
C-556600	-11.7	-24.2	38	0.64	0.59	5.58
C-556601	-11.2	-25.2	14	0.44	0.44	3.85
C-556602	-10.7	-25.1	13	0.36	0.69	4.19
C-556603	-10.2	-24.9	13	0.35	1.13	3.6
C-556604	-9.7	-24.9	13	0.21	0.73	2.5
C-556605	-9.2	-25.5	17	0.35	0.83	4.2
C-556606	-8.7	-25.4	14	0.45	1.01	3.92
C-556607	-8.2	-24.7	16	0.35	0.68	3.69
C-556608	-7.7	-25.6	13	0.32	0.73	3
C-556609	-7.2	-25.0	15	0.37	0.48	3.32
C-556610	-6.7	-24.6	16	0.37	0.63	3.2
C-556611	-6.2	-24.5	13	0.40	0.48	3.42
C-556612	-5.7	-24.3	13	0.29	0.29	3.37
C-556613	-5.2	-24.3	16	0.29	0.45	3.11
C-556614	-4.7	-24.7	9	0.45	0.38	4
C-556615	-4.2	-25.2	14	0.52	0.76	3.22
C-556616	-3.7	-25.2	14	0.24	0.79	2.89
C-556617	-3.2	-25.7	17	0.24	0.84	2.67
C-556618	-3	-25.5	16	0.22	0.72	2.77
C-556619	-3.45	-25.1	15	0.19	2.92	1.66
C-556620	-2.8	-25.3	22	0.40	0.62	4.48
C-556621	-2.6	-25.7	19	0.39	0.82	4.04
C-556622	-2.4	-25.9	18	0.33	0.96	3.84
C-556623	-2.2	-26.1	24	0.39	0.92	3.83
C-556624	-2	-25.6	19	0.41	0.6	3.84
C-556625	-1.8	-25.7	15	0.34	0.8	3.57

C-556626	-1.6	-25.6	17	0.46	0.89	3.9
C-556627	-1.4	-24.8	18	0.35	0.36	4.17
C-556628	-1.2	-25.6	24	0.30	1.14	3.65
C-556629	-1	-25.5	15	0.22	1.31	3.5
C-556630	-0.8	-25.1	18	0.30	0.75	3.82
C-556631	-0.6	-24.5	20	0.29	0.41	3.43
C-556632	-0.4	-24.2	21	0.39	0.77	4.33
C-556633	-0.2	-25.3	16	0.23	0.57	3.42
C-556634	0	-25.5	20	0.33	1.37	3.33
C-556635	1	-29.0	29	0.28	0.48	7.98
C-556636	1.2	-29.6	43	0.24	1.07	8.21
C-556637	1.4	-29.1	48	0.19	1.34	8.69
C-556638	1.6	-28.8	33	0.13	1.21	8.45
C-556639	1.8	-28.6	27	0.14	0.28	8.25
C-556640	2	-28.7	26	0.11	0.52	8.52
C-556641	2.2	-28.8	16	0.10	0.14	8.57
C-556642	2.4	-28.9	20	0.09	0.16	8.57
C-556643	2.6	-30.1	30	0.13	0.46	9.98
C-556644	2.8	-30.4	17	0.10	0.14	7.85
C-556645	2.9	-30.3	25	0.08	0.46	9.5
C-556646	3.1	-30.8	25	0.12	0.17	7.87
C-556647	3.3	-31.0	27	0.22	0.16	8.2
C-556648	3.5	-32.8	41	0.40	0.55	7.96
C-556649	3.7	-32.6	43	0.45	0.96	8.09
C-556650	3.9	-32.5	42	0.43	0.57	8.21
C-556651	4.1	-33.5	77	0.31	4.4	9.75
C-556652	4.3	-32.8	60	0.48	1.59	7.87
C-556653	4.4	-32.6	74	0.27	0.63	8.05
C-556654	5.4	-32.5	62	0.50	1.43	7.99
C-556655	5.6	-32.2	53	0.33	1.23	8.19
C-556656	5.8	-33.3	86	0.42	2.39	9.91
C-556657	6	-32.6	69	0.44	0.76	9.66
C-556658	6.2	-33.2	69	0.31	0.57	9.77
C-556659	6.4	-33.6	60	0.39	1.04	8.47
C-556660	6.6	-33.3	53	0.28	0.48	10.3
C-556661	6.8	-33.2	46	0.26	0.35	10.97
C-556662	7	-32.8	53	0.34	0.44	11.28
C-556663	7.2	-32.6	51	0.34	0.52	10.92
C-556664	7.4	-33.0	50	0.31	0.39	10.76
C-556665	7.6	-32.9	81	0.44	2.76	10.02
C-556666	7.8	-32.9	77	0.56	5.03	8.99
C-556667	8	-32.3	82	0.71	3.91	9.56
C-556668	8.15	-32.7	89	0.51	5.2	7.92

C-556669	8.2	-33.7	134	1.03	20.65	8.74
C-556670	8.4	-33.0	88	0.63	10.16	7.12
C-556671	8.6	-33.5	100	0.61	26.37	7.02
C-556672	8.8	-33.6	57	0.38	4.51	9.62
C-556673	9	-33.8	57	0.41	3.67	9.2
C-556674	9.2	-32.1	25	0.08	1.58	6.99
C-556675	9.4	-33.3	50	0.46	2.77	9.55
C-556676	9.6	-32.8	38	0.25	0.59	10.06
C-556677	9.8	-33.1	26	0.30	0.96	9.54
C-556678	10	-32.9	47	0.23	0.62	10.87
C-556679	10.2	-33.2	35	0.30	1.02	10.63
C-556680	10.4	-33.0	30	0.29	1.92	10.99
C-556681	10.6	-32.8	40	0.49	1.98	9.53
C-556682	10.8	-31.6	19	0.14	1.42	6.76
C-556683	11	-31.8	23	0.17	1.4	9.02
C-556684	11.2	-27.4	74	1.02	1.41	9.1
C-556685	11.4	-31.8	34	0.17	2.14	8.21
C-556686	11.6	-32.1	23	0.21	0.83	9.45
C-556687	11.8	-32.2	31	0.25	1.51	9.31
C-556688	12	-32.6	48	0.39	3.08	9.09
C-556689	12.2	-32.6	56	0.55	2.9	9.23
C-556690	12.4	-31.3	19	0.09	1.28	6.7
C-556691	12.6	-33.1	34	0.29	2.55	9.55
C-556692	12.8	-32.7	35	0.15	3.04	6.67
C-556693	13	-33.1	45	0.33	7.18	7.38
C-556694	13.2	-32.8	47	0.29	4	7.1
C-556695	13.05	-33.9	41	0.48	12.34	9.75
C-556696	13.4	-32.7	34	0.30	4.13	7.19
C-556697	13.6	-33.6	42	0.50	4.96	7.1
C-556698	13.8	-33.3	43	0.48	3.89	7.31
C-556699	14	-32.4	35	0.17	2.55	7.44
C-556700	14.2	-33.4	27	0.31	3.45	4.54
C-556701	14.4	-33.5	24	0.26	3.5	4.57
C-556702	14.8	-32.8	33	0.45	2.31	7.7
C-556703	15.3	-32.4	15	0.18	1.71	7.25
C-556704	15.8	-31.2	10	0.10	0.37	7.99
C-556705	16.3	-31.8	7	0.28	1.53	7.82
C-556706	16.8	-32.4	1	0.35	1.27	7.98
C-556707	17.3	-32.4	1	0.19	3.08	8.2
C-556708	17.8	-25.1	0.43	0.00	3.34	7.79
C-556709	18.8	n.d.	0.49	0.01	3.01	7.72
C-556710	20.3	-31.9	0.36	0.19	3.51	7.98
C-556711	21.8	-32.6	4	0.16	1.32	8.08

C-556712	23.3	-32.5	18	0.64	3.42	7.49
C-556713	24.8	-33.0	20	0.42	2.66	7.43
C-556714	26.3	-32.7	22	0.50	2.96	7.07
C-556715	27.8	-32.7	26	0.54	2.9	7.03
C-556716	29.3	-32.8	25	0.40	1.21	7.42
C-556717	30.8	-32.3	24	0.32	1.36	7.1
C-556718	32.3	-32.8	31	0.73	3.33	7.09
C-556719	33.8	-32.1	34	0.57	2.31	7.16
C-556720	35.3	-31.3	23	0.35	1.04	7.42
C-556721	36.8	-31.8	18	0.49	3.17	7.3
C-556722	38.3	-31.7	9	0.23	0.4	6.65
C-556723	39.8	-31.3	9	0.26	0.8	7.43
C-556724	41.3	-31.3	16	0.30	0.42	7.29
C-556725	44.3	-31.5	22	0.49	0.75	7.38
C-556726	47.3	-31.4	29	0.62	0.71	6.84
C-556727	50.3	-31.1	27	0.45	0.36	7.16
C-556728	53.3	-29.2	9	0.05	0.55	4.44
C-556729	56.3	-29.9	16	0.12	0.42	6.64
C-556730	59.3	-29.7	11	0.15	0.33	6.94
C-556731	62.3	-28.7	10	0.15	0.17	7.56
C-556732	65.3	-29.2	8	0.12	0.29	6.92
C-556733	68.3	-29.8	5	0.07	0.28	6.51
C-556734	71.3	-29.6	8	0.09	0.59	6.67
C-556735	74.3	-29.6	8	0.10	0.46	6.01
C-556736	77.3	-29.5	5	0.06	0.31	6.88
C-556737	80.3	-29.4	7	0.07	0.29	6.66
C-556738	83.3	-29.2	7	0.06	0.26	6.43
C-556739	86.3	-28.6	4	0.04	0.27	6.58
C-556740	89.3	-29.1	14	0.11	0.64	6.84
C-556741	92.3	-28.5	5	0.05	0.19	6.32
C-556742	95.3	-27.9	8	0.13	0.23	6.24
C-556743	98.3	-28.5	5	0.05	0.28	6.36
C-556744	101.3	-28.0	4	0.11	0.24	5.53
C-556745	104.3	-28.3	8	0.05	0.25	5.57
C-556746	107.3	-27.6	3	0.03	0.16	6.66
C-556747	110.3	-28.3	5	0.12	0.25	6.04
C-556748	113.3	-27.6	4	0.02	0.18	5.84
C-556749	116.3	-27.8	12	0.03	0.45	4.94
C-556750	117.8	-28.7	16	0.15	0.85	6.42
C-556751	119.3	-28.3	22	0.16	0.45	6.54
C-556752	122.3	-28.9	16	0.07	0.51	4.1
C-556753	125.3	-27.6	14	0.06	0.3	5.12
C-556754	128.3	-26.7	9	0.04	0.3	5.95

C-556755	134.3	-27.4	10	0.06	0.22	6.44
C-556756	137.3	-27.7	4	0.02	0.16	6.36
C-556757	140.3	-26.8	8	0.04	0.27	6.19
C-556758	143.3	-28.3	30	0.28	0.82	6.06
C-556759	146.3	-27.2	21	0.09	0.27	5.97
C-556760	149.3	-26.7	10	0.08	0.29	6.92
C-556761	152.3	-26.7	16	0.10	0.19	6.55
C-556762	153.3	-26.0	7	0.03	0.25	6.03
C-556763	154.8	-26.0	22	0.11	0.38	6.86
C-556764	157.8	-26.9	10	0.07	0.18	6.32
C-556765	160.8	-27.4	17	0.12	0.27	7.81
C-556766	163.8	-26.8	7	0.02	0.41	6.26
C-556767	166.8	-26.3	9	0.11	0.29	6.92
C-556768	169.8	-26.1	9	0.05	0.22	6.75
C-556769	182.3	-26.5	4	0.04	0.19	5.03
C-556770	196.8	-24.7	7	0.06	0.18	5.23
C-556771	199.8	-25.7	7	0.03	0.14	6.66
C-556772	202.8	-25.7	4	0.02	0.13	6.27
C-556773	205.8	-26.0	4	0.01	0.18	4.37
C-556774	208.8	-26.1	5	0.07	0.16	5.78
C-556775	214.8	-26.0	3	0.01	0.08	5.68
C-556776	217.8	-26.6	5	0.02	0.14	6.88
C-556777	220.8	-27.1	7	0.04	0.11	6.86
C-556778	223.8	-27.4	5	0.02	0.15	6.06
C-556779	226.8	-26.8	5	0.09	0.16	5.99
C-556780	229.8	-27.1	7	0.02	0.18	5.1
C-556781	232.8	-28.7	10	0.05	0.14	5.21
C-556782	235.8	-27.4	10	0.03	0.41	4.33
C-556783	238.8	-27.4	6	0.03	0.18	6.22
C-556784	241.8	-27.7	8	0.06	0.24	6.65
C-556785	244.8	-28.1	11	0.06	0.29	5.71
C-556786	247.8	-29.2	8	0.06	0.2	5.61
C-556787	250.8	-29.4	7	0.06	0.2	6.31
C-556788	253.8	-28.5	5	0.05	0.19	5.81
C-556789	256.8	-31.1	11	0.15	0.32	6.17
C-556790	260.8	-29.7	12	0.09	0.31	6.36
C-556791	263.8	-29.4	9	0.06	0.44	5.57
C-556792	266.8	-31.4	14	0.13	0.3	6.08
C-556793	269.8	-31.6	13	0.19	0.43	5.85
C-556794	272.8	-31.5	15	0.16	0.39	6.14
C-556795	275.8	-28.7	5	0.05	0.14	6.15
C-556796	278.8	-30.2	6	0.10	0.15	5.37
C-556797	281.8	-30.7	5	0.05	0.18	5.13

C-556798	284.8	-31.4	12	0.11	0.62	5.93
C-556799	290.8	-30.1	5	0.06	0.31	5.87
C-556800	293.8	-31.2	15	0.15	1.08	6.6
C-556801	296.8	-31.3	10	0.15	1.09	6.19
C-556802	299.8	-32.5	54	0.50	7.52	6.65
C-556803	302.8	-32.7	55	0.30	10.08	5.56
C-556804	309.8	-32.4	43	0.32	5.94	5.81
C-556805	312.8	-32.9	36	0.23	8.15	4.67
C-556806	315.8	-32.8	65	0.48	11.74	6
C-556807	318.8	-30.6	38	0.43	1.46	6.31
C-556808	321.8	-30.7	32	0.46	1.77	5.93
C-556809	324.8	-30.6	28	0.57	1.54	5.72
C-556810	327.8	-29.9	16	0.28	0.57	5.41
C-556811	330.8	-29.6	23	0.49	0.73	6.23
C-556812	333.8	-30.3	30	0.46	1.55	6.23
C-556813	336.8	-29.6	32	0.61	1.88	6.43
C-556814	339.8	-29.3	11	0.20	0.48	5.07
C-556815	342.8	-28.6	26	0.62	7.48	5.08
C-556816	345.8	-28.7	26	0.91	8.42	6.32
C-556817	348.8	-28.6	18	0.62	3.14	6.27
C-556818	351.8	-28.6	8	0.22	1.44	4.98
C-556819	354.8	-29.1	19	0.93	1.33	6.25
C-556820	357.8	-29.4	19	0.95	0.99	5.79
C-556821	360.8	-29.3	21	1.13	0.83	6.51
C-556822	363.8	-29.1	14	0.66	0.52	6.06
C-556823	366.8	-29.6	13	0.43	2.08	4.21
C-556824	369.8	-30.2	26	0.86	4.3	6.68
C-556825	372.8	-30.5	24	0.80	3.07	6.7
C-556826	375.8	-30.6	19	0.43	2.47	5.69
C-556827	378.8	-30.7	17	0.38	2.11	5.7
C-556828	381.8	-30.5	15	0.25	2.61	5.96
C-556829	387.8	-30.7	12	0.30	2.45	5.74
C-556830	390.8	-30.6	13	0.28	0.8	5.75
C-556831	393.8	-30.4	8	0.23	0.76	4.31
C-556832	396.8	-30.6	10	0.28	0.44	4.86
C-556833	399.8	-30.8	13	0.42	0.79	5.86
C-556834	402.8	-30.5	11	0.34	0.54	5.84
C-556835	405.8	-30.1	6	0.15	0.36	3.72
C-556836	408.8	-30.8	8	0.25	1.1	4.54
C-556837	411.8	-30.8	12	0.28	1.41	4.96
C-556838	414.8	-31.5	20	0.53	3.72	6.7
C-556839	417.8	-31.3	13	0.33	1.99	6
C-556840	420.8	-30.9	13	0.21	1.96	5.37

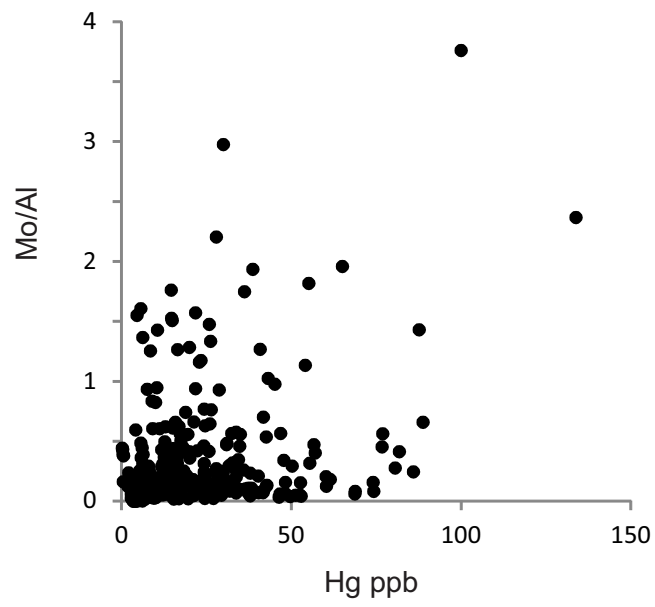|						
C-556841	423.8	-31.5	12	0.37	1.17	5.94
C-556842	426.8	-30.4	6	0.11	1.2	3.86
C-556843	429.8	-31.4	11	0.34	3.49	5.8
C-556844	432.8	-31.0	9	0.26	2.28	3.79
C-556845	435.8	-31.7	17	0.54	6.92	5.49
C-556846	438.8	-31.8	11	0.25	6.32	4.44
C-556847	441.8	-31.2	6	0.19	1.7	3.85
C-556848	444.8	-30.3	4	0.11	1.99	3.37
C-556849	447.8	-31.2	6	0.20	5.56	4.08
C-556850	450.8	-30.9	6	0.22	6.11	3.81
C-556851	453.8	-30.5	8	0.13	2.78	2.99
C-556852	456.8	-31.1	10	0.16	3.47	3.68
C-556853	459.8	-29.7	4	0.07	0.66	4.23
C-556854	462.8	-30.4	6	0.10	1.8	3.73
C-556855	468.3	-28.4	7	0.11	0.25	4.19
C-556856	475.3	-29.6	5	0.10	1.23	4.87
C-556857	479.8	-30.2	7	0.11	0.45	4.62
C-556858	482.8	-30.3	7	0.14	0.55	4.04
C-556859	485.8	-29.5	8	0.14	0.75	4.93
C-556860	488.8	-28.5	3	0.05	0.22	3.78
C-556861	491.8	-29.8	7	0.12	0.42	4.09
C-556862	499.8	-30.0	7	0.24	0.63	3.98

445

Grasby et al. Figure 1
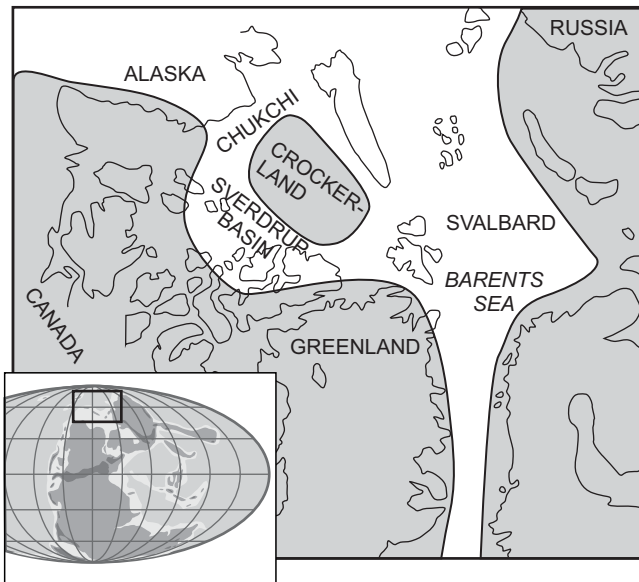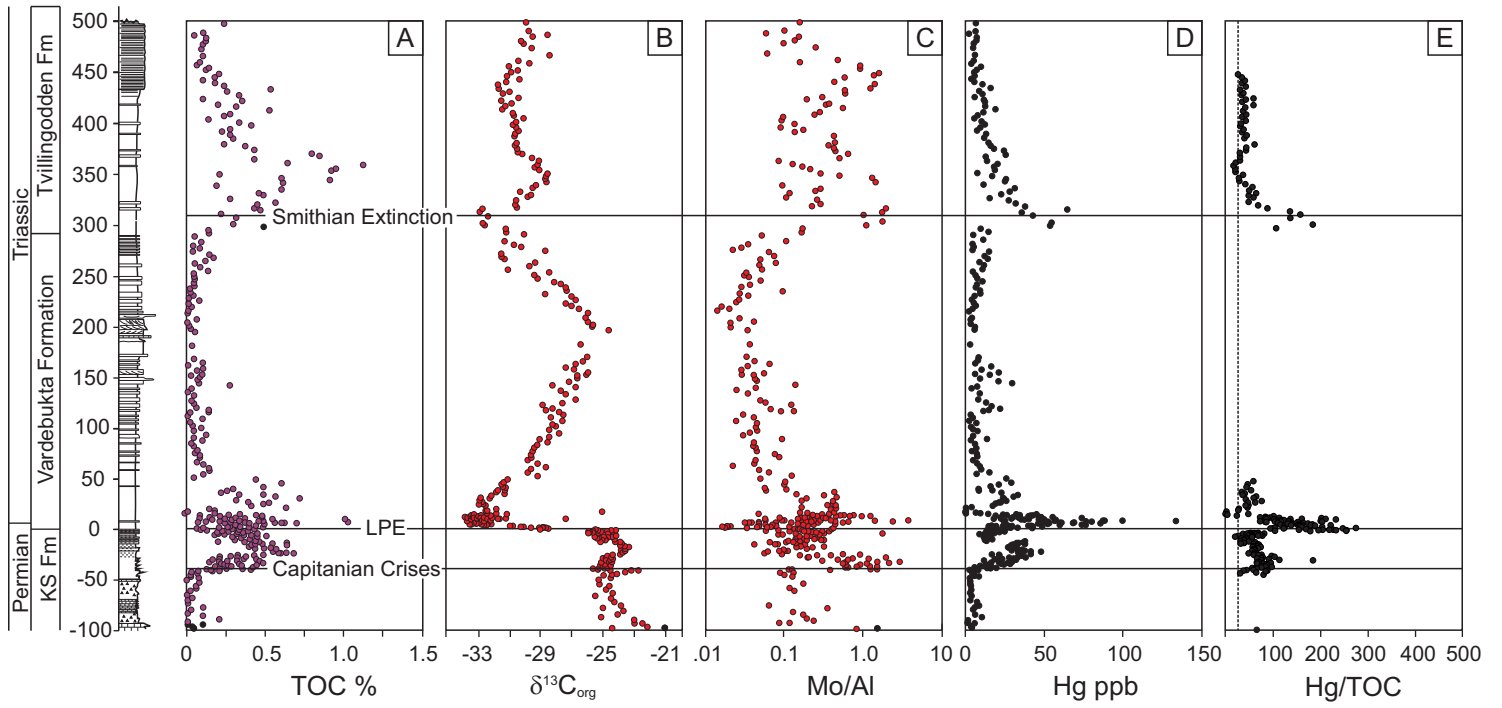
Grasby et al. Figure 3
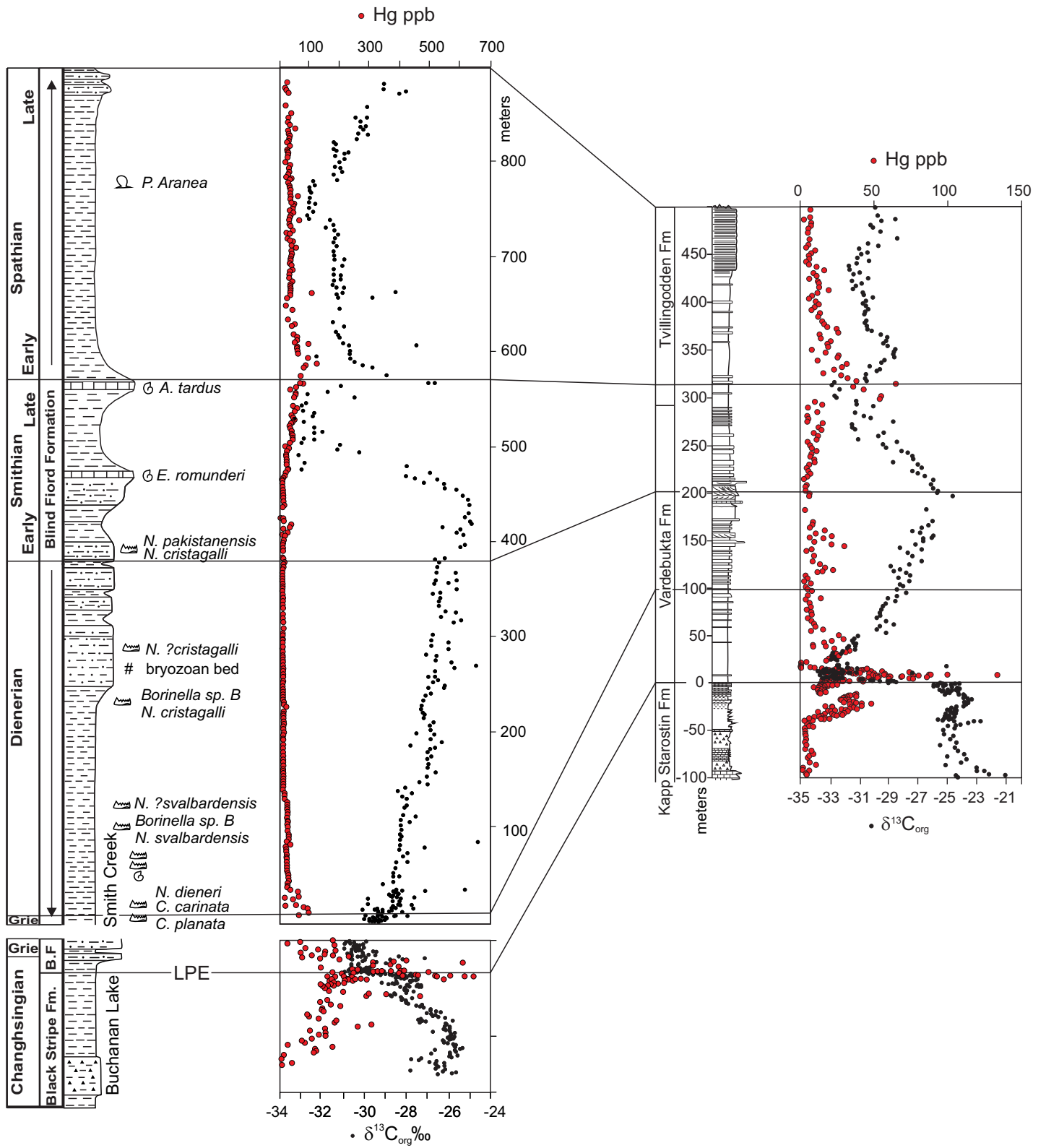
Grasby et al. Figure 4

Grasby et al. Figure 5